Multistable metafluid based energy harvesting and storage

Ofek Peretz Ezra Ben Abu Anna Zigelman Sefi Givli Amir D. Gat*

Dr. O. P., E. B., Dr. A. Z., Prof. S. G., Prof. A. G.
Faculty of Mechanical Engineering, Technion - Israel Institute of Technology, Haifa, 3200003, Israel
Email Address: ofekperetz@technion.ac.il

Keywords: *Multistability, Metafluid, Energy Harvesting*

The thermodynamic properties of fluids play a crucial role in many engineering applications, particularly in the context of energy. Fluids with multistable thermodynamic properties may offer new paths for harvesting and storing energy via transitions between equilibria states. Such artificial multistable fluids can be created using the approach employed in metamaterials, which controls macro-properties through micro-structure composition. In this work, the dynamics of such 'metafluids' is examined for a configuration of calorically-perfect compressible gas contained within multistable elastic capsules flowing in a fluid-filled tube. We study both analytically and experimentally the velocity-, pressure-, and temperature-fields of multistable compressible metafluids, focusing on transitions between different equilibria. We first examine the dynamics of a single capsule, which may move or change equilibrium state, due to fluidic forces. We then study the interaction and motion of multiple capsules within a fluid-filled tube. We show that such a system can be used to harvest energy from external temperature variations in either time or space. Thus, fluidic multistability allows specific quanta of energy to be captured and stored indefinitely as well as transported as a fluid, via tubes, at standard atmospheric conditions without the need for thermal isolation.

1 Introduction

The development of clean and efficient heat engines, refrigeration, energy storage, and energy harvesting is one of humanity's most pressing challenges today. The emission associated with these cycles is a primary contributor to global warming, and the use of hazardous fluids, required for efficient cooling cycles, makes refrigeration the world's current most polluting technology [1, 2, 3, 4]. This motivates the development of new fluids with enhanced thermodynamic properties that enable cleaner and more efficient energy cycles.

As a step in this direction, we propose fabricating a new class of fluids, namely artificial fluids that exhibit multistable thermodynamic properties. Our aim is to take the knowledge gained in creating multistable metamaterials, where extraordinary macroscale behaviors have been enabled through careful design of microscale architecture, and extend it to the creation of multistable fluids.These metafluids are created by suspending multistable architected capsules, each enclosing a compressible gas, in a lubricating fluid [5]. The multistable thermodynamic properties of such metafluids offer new and exciting opportunities for the storage and harvesting of energy. In both refrigeration and heat engine cycles, fluids are transported between hot and cold regions, as well as between high- and low-pressure areas. Thus, clearly, any attempt to incorporate multistable metafluids in such cycles requires an understanding of the transport phenomena of such fluids. Consequently, effects such as compression, expansion, time-dependent flow field, and heat transfer to the encapsulated gas, must be accounted for. Here, we aim to study, in terms of exergy, the effects of these phenomena on the ability of the multistable fluid to harvest, store, and release energy.

The concept of a suspension of multistable capsules draws inspiration from multistable mechanical metamaterials. Metamaterials are architected structures, often consisting of periodically arranged building blocks that deform, rotate, buckle, fold, or snap in response to mechanical stimuli. A careful design of the micro-level architecture enables metamaterials to provide exceptional macro-behavior, properties, and functionalities that surpass those of standard materials [6]. For more than two decades, metamaterials that manipulate optical [7, 8], acoustic [9], and thermal [10] fields as well as stress waves [11, 12, 13], and that have highly unusual properties, such as a "negative mass" [14, 15, 16] or ultra-high stiffness to weight ratio [17] have attracted a great deal of attention. Multistable metamaterials, consisting of an array of bistable units, are a promising class of mechanical metamaterials. They are characterized by a multitude of possible equilibrium configurations, for a prescribed load, that differ in the state of each building block, thus leading to a highly inhomogeneous and non-affine deformation field for the whole body [18]. It has been demonstrated that the highly non-convex energy landscape associated with these materials provides unusual behaviors, including super-elasticity, mechanical memory, large reversible deformations, and efficient dissipation, all of which are highly useful for engineering applications such as soft robotics,

This article has been accepted for publication and undergone full peer review but has not been through the copyediting, typesetting, pagination and proofreading process, which may lead to differences between this version and the Version of Record. Please cite this article as doi: 10.1002/adma.202301483

vibration mitigation, energy absorption, and phase-transforming smart materials [19, 20, 21, 22, 23, 24, 25, 26].

In order to use multistable metamaterials in energy cycles, one has to enable their transport. This leads to the concept of multistable metafluids, namely artificial suspensions that include a mixture of a standard fluid and architected multistable capsules, engineered to give rise to exceptional thermodynamic properties that extend beyond those of naturally available fluids [5, 27]. For example, Epstein *et al.* [28] have designed colloidal particles that rapidly and reversibly snap between two bistable shapes. This shape change occurs inside a fluid by altering its pH, on an extremely short timescale which enables to decouple the particles' shape change from the diffusion-limited stimulus trigger. Generally, different liquid materials including water, liquid crystal, and liquid metals may be used for realizing the metafluidic metamaterials. The large choice (of properties) of the liquid background combined with the tunability offered by the metamaterial particles promise relevance to a wide range of applications, from material sensing and bio-detection to energy harvesting and imaging [29].

Recently, Peretz *et al.* [5] studied the steady state thermodynamic properties of a metafluid which was composed of a multitude of multistable gas-filled capsules suspended in a liquid, where each (bi-stable) element of the capsule was comprised of two non-identical conical frusta in opposing orientations. Central to this research was the definition of a *permutation*, which refers to a state-vector containing the number of the capsule's elements in each of the two phases (open and close) and the spinodal region (partially open). We adopt a similar nomenclature in the current study, and while Peretz *et al.* [5] examined the steady state thermodynamics, we here focus on transient energy harvesting processes and the induced flow of the metafluid. To this end, we study a simple, yet practical, case of gas-filled multistable capsules lubricated by an external fluid and contained within a closely-fitted tube.

2 Results

In this work, we study dynamics due to the flow, compression and expansion of a metafluid made of multistable capsules enclosed within a closely fitted, liquid-filled tube. These dynamics are determined by the interaction between the capsule properties, gas thermodynamics, and flow of the external lubricating liquid. The capsules compress, expand or switch between equilibria branches, due to external changes in temperature and pressure in both isobaric and isentropic processes. Each capsule in the current study is composed of n identical bi-stable elastic elements, creating a single encapsulated volume filled with a compressible gas. Each element of the capsule is composed of two non-identical conical frusta in opposing orientations. Bi-stability is achieved by switching between extended and collapsed states, through inversion of one frustum, thus yielding a significant change in the internal element volume. The bistable behavior and related kinematics of simple conical frusta were studied in detail in [30, 31, 32, 33]. The overall pressure-volume relation of the capsule is determined by the number of elements in phase I (n_{I}), in phase II (n_{II}), and in the spinodal (n_s). For convenience, hereafter, we denote the vector containing the number of elements in each multistable state as the permutation, $\overrightarrow{\mathbf{per}} = \{n_{\mathrm{I}}, n_s, n_{\mathrm{II}}\}$.

2.1 Illustrating a multistable energy harvesting cycle

Figure 1 illustrates the key thermodynamics of the the proposed cycle, consists of three phases:

I. Energy absorption: The system is initially at atmospheric conditions ($T_1 = T_{\mathrm{atm}}$, $p_1 = p_{\mathrm{atm}}$), and the initial permutation can be chosen from the set of all possible stable permutations. The system is then exposed to high temperature ($T_2 = T_{\mathrm{hot}}$) causing the encapsulated air within the capsules to expand. Due to the multistable nature of the structure, the capsules snap to the first stability branch whose snapping-up temperature exceeds that of the system. The temperature is then reduced back to the nominal value ($T_3 = T_{\mathrm{atm}}$) and the capsule's permutation is determined by the last stability branch whose snapping-down temperature is lower than the ambient temperature. As seen in Figure 1c, the multistability of the capsules and the associated hysteresis cause a difference in the capsule volume between states (1) and (3), while both the pressure and temperature values are identical, representing the charging process of the system.

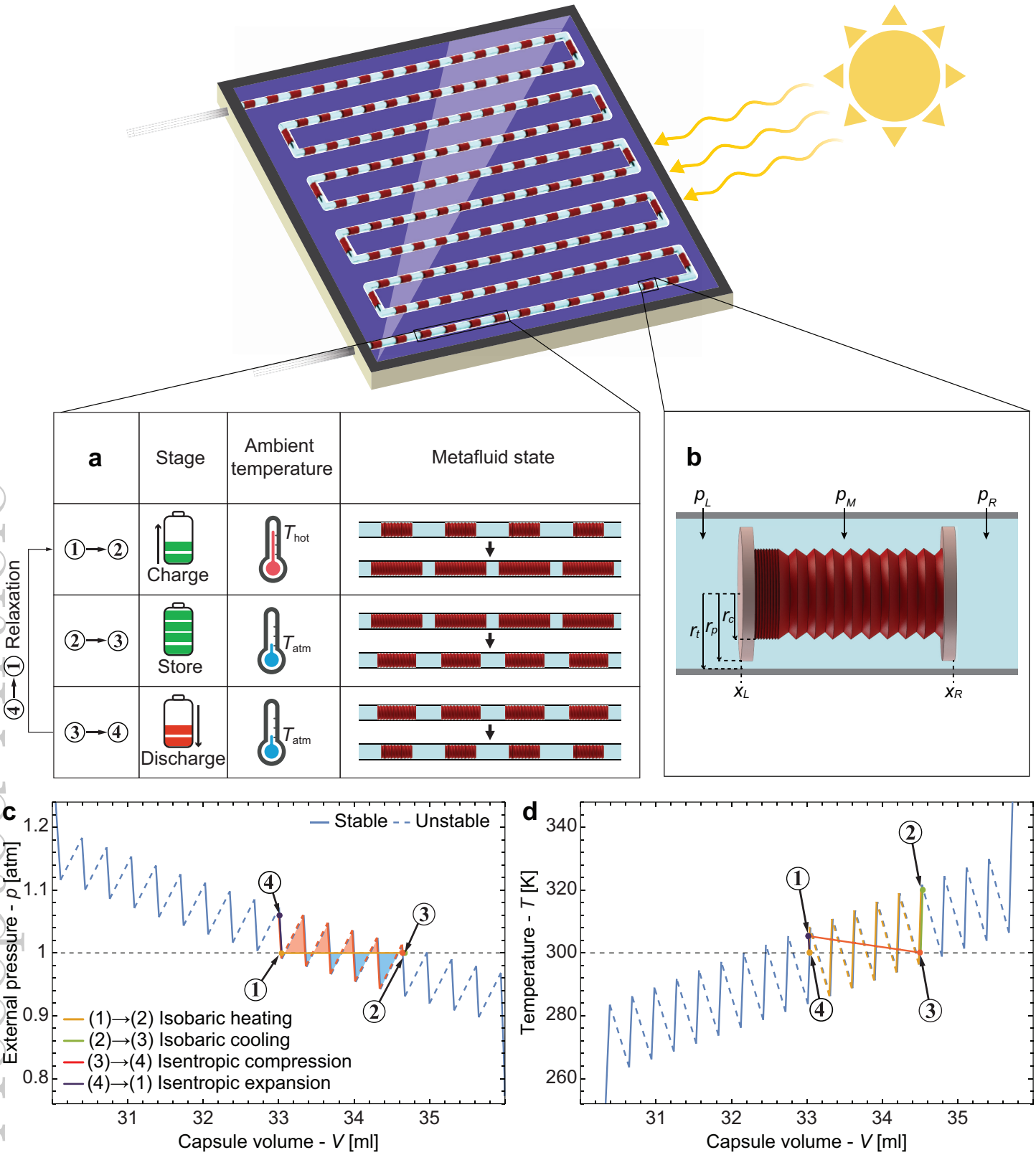

Figure 1: **An illustration of an energy harvesting and storing device based on a multistable metafluid.** **a**, Schematic description of thermodynamic processes for energy harvesting and storage: (1)→(2) By heating isobarically, the metafluid is transferred to a higher energy equilibrium branch. (2)→(3) After being isobarically cooled back to its original temperature, the metafluid remains at a higher-energy equilibrium branch, which allows for the storage of energy in the metafluid. (3)→(4) Isentropic compression extracts energy from the metafluid, resulting in a transfer to a lower energy equilibrium branch. (4)→(1) Relaxation by isentropic expansion, while the metafluid remains in the lower energy equilibrium branch. **b**, A detailed view of a multistable, gas-filled capsule. **c**, External pressure versus capsule volume for isentropic processes. **d**, Temperature versus capsule volume for isobaric processes, where the solid and the dashed blue lines represent stable and unstable equilibrium branches, respectively, and the dashed black line represents atmospheric conditions.

II. Energy storage: The energy absorbed within the system is now stored at a stable equilibria point of the capsules in the form of expanded gas and elastic strain energy while the system is at atmospheric conditions (both temperature and pressure). This represents a key characteristic of the proposed system, as it eliminates the need of thermal isolation and efficiency loss over time. Moreover, the charged capsules can be transported to a desired location in which the energy can be harvested.

III. Energy extraction: To discharge the stored energy from the system, high pressure is applied (denoted by (3)→(4) isentropic compression), causing the capsules to contract and snap-down until reaching a stable permutation (the pressure is chosen to allow the system to return to its initial permutation) releasing the stored energy in the form of mechanical work. Finally, the pressure is returned to its initial value (denoted by (4)→(1) isentropic expansion), thus returning the system to its initial state, thereby allowing cyclic operation (see Figure 1d).

By harnessing the multi-stability of the capsules, the metafluid can hold multiple stable energetic states under at the same pressure and temperature conditions. This unique property allows for the transport of energy quanta (or heat) in atmospheric conditions without necessitating thermal insulation or gas pressurization. Consequently, our approach offers distinct advantages over standard working fluids in traditional cycles, such as the Otto and Brayton cycles.

2.2 Single capsule properties

This work focuses on non-equilibrium dynamics of metafluids; yet, it is instructive to first present multi-stable energy harvesting cycle based on steady-state equilibria of a single capsule (see detailed steady-state analysis in [5]). To this end, we examine a capsule without external forces, with the exception of a uniform external pressure p, and internal pressure p_{gas} of the encapsulated gas. We begin by defining the elastic tension (denoted as f_e) - volume (denoted as v_i) relation of a single element within a capsule. For simplicity, and following [34] and [35], we approximate this relation by a tri-linear approximation. The tri-linear curve is defined by the stiffnesses k_{I} and k_{II}, and the stability threshold points $(v_s^{\text{I}}, f_s^{\text{open}})$ and $(v_s^{\text{II}}, f_s^{\text{close}})$ in phases I and II, respectively. The spinodal (negative) stiffness k_s is determined by requiring continuity between the spinodal region and phases I and II, yielding $k_s = (f_s^{\text{close}} - f_s^{\text{open}})/(v_s^{\text{II}} - v_s^{\text{I}}) < 0$, resulting in

$$f_e = \begin{cases} k_{\text{I}}\left(v_i - v_s^{\text{I}}\right) + f_s^{\text{open}} \\ k_s\left(v_i - v_s^{\text{I}}\right) + f_s^{\text{open}} \\ k_{\text{II}}\left(v_i - v_s^{\text{II}}\right) + f_s^{\text{close}} \end{cases}, \quad \begin{matrix} v_i < v_s^{\text{I}} \\ v_s^{\text{I}} < v_i < v_s^{\text{II}}, \\ v_s^{\text{II}} < v_i \end{matrix} \quad \begin{matrix} \text{Phase I (stable)} \\ \text{Spinodal (unstable).} \\ \text{Phase II (stable)} \end{matrix} \tag{1}$$

Next, we address the total gas-filled volume of a capsule, which is composed of the sum of all volumes of the n bi-stable elements (given by $\sum_{i=1}^{n} v_i$). Note that the tension acting on all elements is identical, and the overall tension-volume relation of the capsule for a given tension f_e is dictated only by the number of elements in phase I (n_{I}), in phase II (n_{II}), and in the spinodal (n_s), yielding

$$v_{\text{tot}} = \overrightarrow{\mathbf{per}} \cdot \left\{ \frac{f_e - f_{\text{s}}^{\text{open}}}{k_{\text{I}}} + v_{\text{s}}^{\text{I}}, \frac{f_e - f_{\text{s}}^{\text{open}}}{k_{\text{s}}} + v_{\text{s}}^{\text{I}}, \frac{f_e - f_{\text{s}}^{\text{close}}}{k_{\text{II}}} + v_{\text{s}}^{\text{II}} \right\}. \tag{2}$$

The value of the elastic tension f_e is affected by external forces (due to other capsules), as well as the internal gas contained within capsule. The encapsulated gas is assumed to be ideal and calorically-perfect and, therefore, the pressure-volume relation is $p_{\text{gas}} = m_{\text{gas}}RT/v_{\text{tot}}$ for an isothermal process or $p_{\text{gas}} = m_{\text{gas}}RT/v_{\text{tot}}^{\gamma}$ for an isentropic process, where R is the specific gas constant, T is temperature, m_{gas} is the mass of the gas within the capsule, and γ is the adiabatic index. Note that Equation (2) implies that several permutations are possible for a prescribed volume of the capsule (see also Figure 1c). This feature is of fundamental importance as further described below.

2.3 Dynamics of multiple capsules

We now turn to examine the dynamics occurring for multiple capsules. We start by formulating the governing equations for each capsule and proceed to present the equations for interaction with adjacent

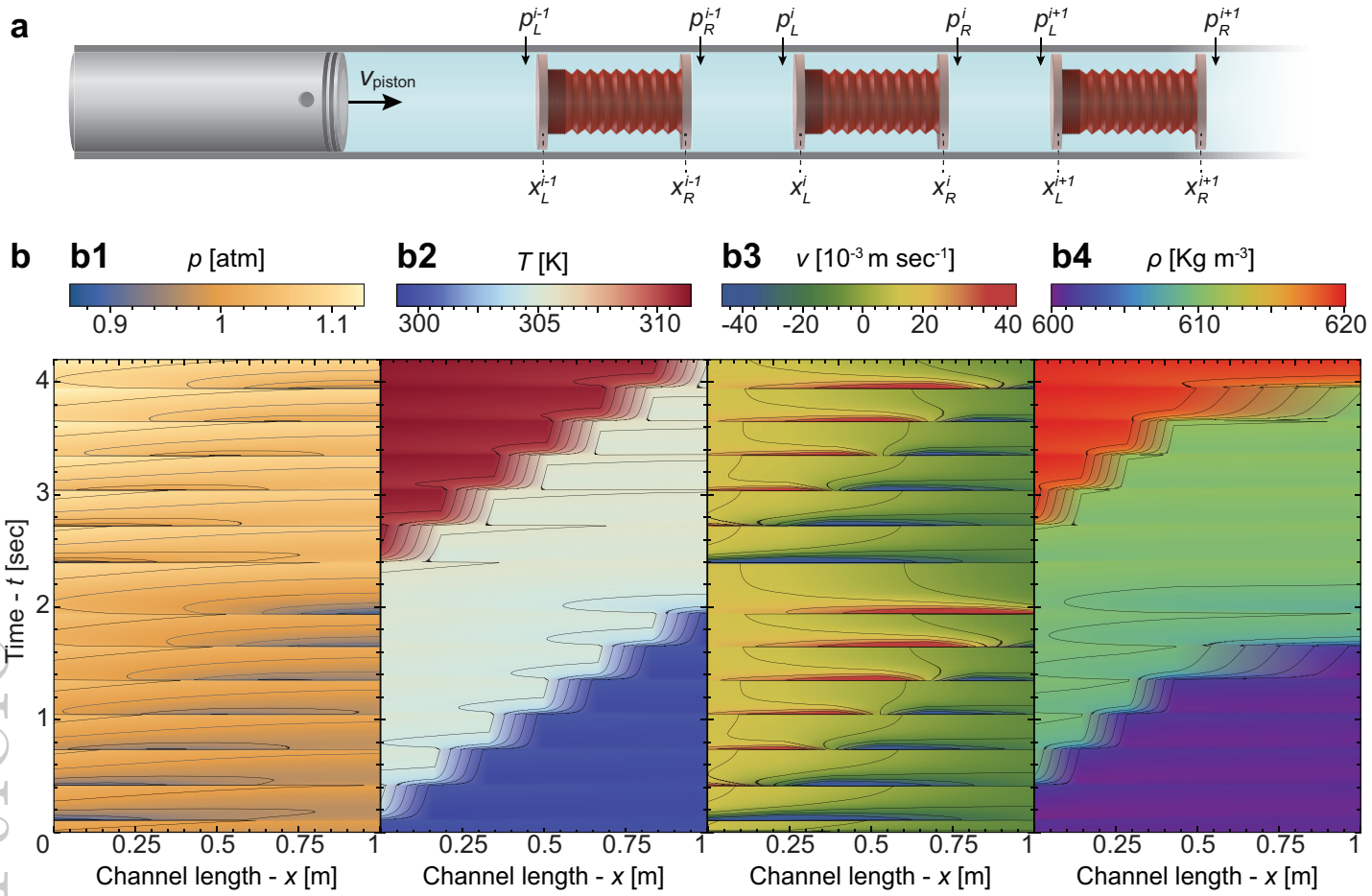

Figure 2: **Analytical results for the energy discharge process. a**, A schematic illustration of metafluid composed of a 1D array of lubricated multistable capsules. The capsules are initially at a high-energy permutation ($\overrightarrow{\mathbf{per}} = \{7, 0, 11\}$), and at $t = 0$ sec, a piston (or fluid) is inserted at a constant velocity, forcing the capsules to contract. In response to this compression, fluidic pressure along the channel gradually increases. When the pressure exceeds a critical value, the capsule snaps, causing a sudden drop in fluidic pressure, which affects neighboring capsules. **a**, fluidic pressure (**b1**), temperature (**b2**), velocity (**b3**) and density (**b4**) along the tube (horizontal axis) versus time (vertical axis). When snapping occurs, the pressure around the capsules drops below the nominal pressure (p_{atm}), pulling adjacent capsules to fill the gap. As can be seen in the Figure, there are two dominant time scales. The slow time scale relates to the propagation rate of information within the tube, while the fast time scale refers to the snapping dynamics that occur during the transition between permutations.

capsules. For each capsule, we denote the pressure at its left and right sides by p_L and p_R, respectively, and the locations of the left and right sides are x_L and x_R, respectively (see Figure 1b). The dynamic response of the individual capsule is strongly influenced by that of the other capsules through the surrounding liquid. The multistable capsule dynamics are governed by several factors, including the movement of the capsule, its compression or expansion, and the fluidic flux that flows over and around it, which is governed by the movement and compression of adjacent capsules. In order to have similar characteristic time- and length-scales of all effects, as well as for slowing down and thus allowing experimental observation of these dynamics, cylindrical plates of radius r_p and width w are attached to each side of the capsule to increase viscous resistance. Force balance on each side of the capsule yields two force relations

$$p_L(t)\pi r_p^2 - F_c\left(v(t), t\right) - F_{\mu,L}(t) - p_M(t)\pi(r_p^2 - r_c^2) = 0, \tag{3a}$$

$$-p_R(t)\pi r_p^2 + F_c\left(v(t), t\right) - F_{\mu,R}(t) + p_M(t)\pi(r_p^2 - r_c^2) = 0 \tag{3b}$$

and mass balance yields

$$Q_L - Q_R = 2\pi r_t(r_t - r_c)\left(\frac{\partial x_R}{\partial t} - \frac{\partial x_L}{\partial t}\right), \tag{4}$$

where $p_M(t)$ is the the pressure between the edges of the capsule, Q_L and Q_R are the fluidic fluxes going over the left and right sides of the capsules respectively (see Figure 1b).The assumptions of negligible inertia and slender geometry allow calculation of the viscous force $f_{\mu,L}$ (and $f_{\mu,R}$) appearing in Equation (3), which yields

$$f_{\mu,L} = \frac{2\pi r_p w\mu}{r_t - r_p}\left[\frac{\partial x_L}{\partial t} + \frac{(r_t - r_p)^2}{2\mu w}\left(p_M(t) - p_L\right)\right], \tag{5}$$

where w and r_p are the width and radius of the plate, r_t is the radius of the tube, r_c is the radius of the capsule, and μ is the viscosity of the fluid. Solving Equation (5) requires obtaining an expression for the mass fluxes, which are given by lubrication approximation as

$$Q_L = 2\pi r_t\left(\frac{(r_t - r_p)^3}{12\mu}\frac{p_L(t) - p_M(t)}{w} - \frac{r_t - r_p}{2}\frac{\partial x_L}{\partial t}\right). \tag{6}$$

(See detailed derivation, as well as the expression for Q_R in Supplementary Note 1.)

For the case of 1D-lattice of N capsules the variables defining each capsule are x_L^i, x_R^i, p_L^i, p_R^i, where $i \in \{1, 2, ..., n\}$ ($i = 1$ denotes the first capsule near the inlet and $i = N$ denotes the capsule closest to the outlet), resulting in $4N$ variables. The above force balance (Equation (4)) and mass conservation (Equation (5)) yield $2N$ equations. Additional relations are obtained from mass and momentum balance in the region between adjacent capsules. Assuming that the viscous resistance between the capsules is negligible compared to the viscous resistance of the plates attached to the capsules, we get that there is no pressure gradient within the gaps, $p_L^i = p_R^{i-1}$, for $i = 2, \dots N$. Requiring mass conservation in the gaps between the capsules, we get that

$$Q_L^i - Q_R^{i-1} = \pi r_t^2\left(\frac{\partial x_R^{i-1}}{\partial t} - \frac{\partial x_L^i}{\partial t}\right), \quad i = 2, \dots, N, \tag{7}$$

which yields a total of $2N - 2$ relations. To fully define the system, two additional relations are obtained from the boundary conditions at the inlet and the outlet of the tube. At the inlet, a piston is inserted in a constant and known velocity, denoted by v_{piston}, namely $\partial x_1/\partial t = v_{\text{piston}}(t)$ and the outlet is closed, yielding $Q_R^N = 0$.

This system of $4N$ equations is to be solved using a set of initial conditions, $p_L^i(t = 0) = p_R^i(t = 0) = p_{atm}$, and $x_L^i(t = 0) = 0.5(i - 1)\Delta x + 0.5(i - 2)l_0$, $x_R^i(t = 0) = 0.5(i - 1)\Delta x + 0.5il_0$, where Δx is the initial gap between capsules and l_0 is the initial length of the capsules, determined by the capsules volume at state (3) of the cycle. The above set of $4N$ equations describes the interaction of the internal gas with the multistable structure and the external fluid, resulting in a pressure-temperature-volume relation that determines both the dynamics and stability states of each capsule. For a given permutation, this relation is defined. A transition between permutations occurs when the tension f_e increases above f_s^{open} or decreases below f_s^{close}, due to a change of temperature or compressive force (see Figure 1c and 1d). The transition between different permutations is associated with different capsule volumes at atmospheric conditions. This results in a change in the internal energy values of both the gas and the elastic structure. As a result, thermal energy can be absorbed by the encapsulated gas, stored within the system, and released when needed.

In **Figure 2**, we show the compression dynamics of a 1D metafluid within a slender tube, based on the solution of Equation (1)-(7). Our calculation begins at stage (3) of the energy cycle (see Figure 1d), which means that the capsules have already been exposed to a high temperature (or another energy source) and have subsequently been transferred to a high-energy permutation before being cooled to the nominal temperature. The physical parameters used for this simulation are: $r_t = 16$ mm, $r_p = 15.5$ mm, $r_c = 15$ mm, $w = 6$ mm, $\mu = 60$ Pa sec, $\Delta_x = 2$ mm, $f_s^{\text{close}} = -11.74$ Pa m^2, $f_s^{\text{open}} = 18.54$ Pa m^2, $l_0 = 0.067$ m, $v_{\text{s}}^{\text{I}} = 0.26$ ml, $v_{\text{s}}^{\text{II}} = 1.04$ ml, $k_{\text{I}} = 1.68$ N ml^{-1}, $k_{\text{II}} = 0.11$ N ml^{-1}. The capsules are initially exposed to high temperature ($T_{\text{hot}} = 320$ K). Thus, initially, all of the capsules are at permutation $\overrightarrow{\mathbf{per}} = \{6, 0, 12\}$, rather than at the minimal energy permutation which is $\overrightarrow{\mathbf{per}} = \{9, 0, 9\}$ (denoted hereafter as atmospheric permutation). In this permutation the pressure of the internal gas equals the external pressure, and thus the

internal exergy is zero. A Mathematica code solving this system of equations is provided in Supplementary Software 1.

In the simulations presented in Figure 2, the metafluid is compressed by a piston entering into the tube, thus transferring the capsules between different equilibria permutations while creating flow dynamics.

The compression of the system results in a pressure increase throughout the tube and therefore causes compression of the capsules. When the elastic tension of the capsule reaches a critical value (f_s^{close}), the capsule snaps and stabilizes in a new permutation. The sudden decrease in volume affects the flow field around the snapping capsule, which in turn affects the neighboring capsules' volume and speed. More specifically, in Figure 2b1, we show the pressure field along the tube (horizontal axis) evolving in time (vertical axis). As seen in the Figure, there are two dominant time scales. The slow time is the rate of snap-through sequence propagation, which can be estimated by the ratio between the time it takes for a capsule located along the tube to snap by its distance from the inlet. The fast time scale is the snapping dynamics occurring during transition between permutations.

Further, the results show a peculiar characteristic not found in naturally available fluids, since a negative gauge pressure is induced when in response to compression of the system, due to the transition between stability branches of the capsules' elements. Figure 2b3 shows the velocity field throughout the tube (horizontal axis) evolving in time (vertical axis). As seen in the figure, snap-close events attract the neighboring capsules towards the snapping capsules, creating a positive velocity before the snap and a negative velocity afterwords, affecting nearly all capsules in the system. The sudden changes in pressure and velocity result in similar behavior regarding density and temperature, as shown in Figure 2b2 and 2b4.

2.4 Experimental demonstration

To verify the analysis and the resulting characteristics of a 1D metafluid flow-field, an experimental setup was fabricated. The experimental setup (**Figure 3a**) consists of a slender Polymethyl methacrylate (PMMA) tube (inner radius 3.2 cm, outer radius 4.1 cm, length $L = 100$ cm) connected on both sides to fluid reservoirs containing Silicon oil (dynamic viscosity $\mu = 60$ Pa sec). Each of the fluidic reservoirs is connected to a pressure controller (Elveflow OB1, see Supplementary Note 2 for technical details) at the inlet ($x = 0$ m) and at the outlet ($x = 1$ m). The tube contains capsules composed of $n = 18$ bistable elements, and the physical parameters of the capsules were measured experimentally, yielding: $v_{\text{s}}^{\text{I}} = 0.26$ ml, $v_{\text{s}}^{\text{II}} = 1.04$ ml, $k_{\text{I}} = 2300$ N ml^{-1}, $k_{\text{II}} = 152$ N ml^{-1}, $f_s^{\text{close}} = 84.4138$ Pa m^2, $f_s^{\text{open}} = -53.4342$ Pa m^2, with standard deviation of ± 0.3217 Pa m^2 (see Supplementary Note 3 for details). The capsule's velocity, length, and position were measured using a in-house video analysis code (see Supplementary Software 2 as well as measurement error analysis provided in Supplementary Note 2) allowing us to analyse the propagation of pressure throughout the metafluid, its effect on the individual capsules, and their interconnected behaviour.

Using this experimental setup, we investigate the system's response to external temperature and pressure variations. Initially, all capsules were set to the same permutation of $\overrightarrow{\mathbf{per}} = \{9, 0, 9\}$, indicative of nominal conditions (state (1)). The system was then exposed to a high temperature by pre-heating the fluidic reservoir connected to the outlet and allowing the heated fluid to flow into the system at $t = 0$ sec. Throughout the experiment, both reservoirs were maintained at atmospheric pressure. Figure 3b showcases the experimental results (Figure 3b1 - temperature measurements at $x = 0.5$m, Figure 3b2 - capsules' location vs time, and Figure 3b3 - capsules length vs time), while Figure 3e illustrates the system state at various time intervals. In this experiment, the temperature was increased to 325 K for 40 seconds, followed by the removal of the heat source, enabling the system to cool back to near ambient temperature. As observed in the figure, at the end of this stage, the capsules remained in a higher permutation of $\overrightarrow{\mathbf{per}} = \{6, 0, 12\}$, signifying a high-exergy state (stage (3) in Figure1).

After the system cooled down to room temperature, we continued the experiment as depicted in Figure 3c1, by introducing a Heaviside pressure function of $p = 3$ atm at the inlet with a duration of 3 seconds. Figure 3c1 shows pressure measurement at the inlet as a function of time, highlighting the actual pressure profile at the inlet (this profile was also employed in the theoretical model for a more realistic comparison. Figure 3d presents the system state at different times, in along with the video analysis results. Figure 3c1

c2 provides a comparison between the model (dashed line) and experimental results (solid line).

While this experiment demonstrates energy charge and discharge in a closed system, it is also possible to release stored energy in an open system, while allowing flow throughout the system. To illustrate this case, we repeated the experiment with the outlet ($x = 1$ m) open to atmospheric pressure without a zero flux requirement at the outlet. Experimental results for this case are provided in Supplementary Movie 2 and Supplementary Note 4.1. In addition, a gradual pressure loading experiment was conducted to show transition between stability brunches and viscosity settling time characteristics. Experimental results for this case are provided in Supplementary Movie 3 and Supplementary Note 4.2.

2.5 Properties of energy harvesting cycles

2.5.1 Extracted energy calculation

The theoretical model derived above can now be used to calculate the amount of energy that is extracted from the system during the discharge stage of the cycle. As previously discussed, energy is introduced to the system via variations in ambient temperature (either in location or in time), and is stored in the form of elastic strain and compressed gas. Energy is extracted by inserting a piston at the inlet, at a constant velocity. The work done by the piston on the system is given by

$$W(t) = \int_0^t \left(p_L^{i=1}(\tilde{t}) - p_a\right) \pi r_t^2 V_{\text{piston}} d\tilde{t}, \tag{8}$$

where $\pi r_t^2 V_{\text{piston}} d\tilde{t}$ denotes the differential amount of volume introduced into the system. The additive volume introduced into the system causes all capsules to be compressed gradually, until one capsule reaches its volume threshold point, and snaps to a lower-volume permutation. This transition between permutations yields a negative gauge pressure around the capsule, thus decreasing the pressure acting on the piston below atmospheric pressure. According to Equation (8), this temporal pressure reduction results in a negative work value ($W(t) < 0$), indicating that the system performs work on the piston, converting the stored energy into mechanical energy.

In **Figure 4** we present energy discharge of the stored energy within the metafluid. In all cases, the capsules begins at a high energetic state ($\overrightarrow{\mathbf{per}} = \{5, 0, 13\}$) and the piston is moving at a constant velocity. The actuation duration is determined by requiring that the capsule's volume at the end of the cycle returns back to atmospheric permutation ($\overrightarrow{\mathbf{per}} = \{9, 0, 9\}$). Figure 4a shows work done on the system in the discharging process versus time at various piston velocities in the range of $v_{\text{piston}} \in [3, 20]$ m sec^{-1}. To extract the stored energy, we first need to increase the system energy above the energetic barrier, denoted by E_{in} (see inset in Figure 4a), which allows to release the energy stored within the structure, denoted by E_{out}. As seen in the Figure, when the velocity increases, the net extracted energy (denoted by $W(t)$) decreases since a higher velocity creates a stronger viscous friction, increasing energy dissipation. Specifically, Figure 4a1 and a2 show inlet pressure as a function of time for the case of $v_{\text{piston}} = 20$ m sec^{-1} and $v_{\text{piston}} = 3$ m sec^{-1}, respectively (blue areas denotes negative gauge pressure and and red areas denotes positive gauge pressure).

As mentioned above, slower piston velocity reduces viscous frictional effects, increasing discharge process efficiency. It does, however, increase the actuation time of each cycle, which could be significant for large numbers of harvesting cycles. To determine the optimal piston velocity, we measure the energy extraction rate (Power), as the total amount of energy extracted from the system in a single cycle (denoted by ΔW) divided by the cycle duration (denoted by $\Delta t_{\text{actuation}}$). Figure 4b shows power (P) versus piston velocity (v_{piston}) for different viscosities of lubricating fluid. Optimal velocity (denoted by $\times$ in the Figure) is determined by the highest energy extraction rate for a given viscosity. As seen in the Figure, lower viscosity yields higher optimal actuation velocity. It is also important to note that with a decrease in viscosity, a greater amount of energy can be discharged from the system, representing an important design rule.

The efficiency of the system can be further enhanced by optimizing the operation range in terms of capsule volume. As discussed in Section 2.1, there are several stable permutations available at each stage

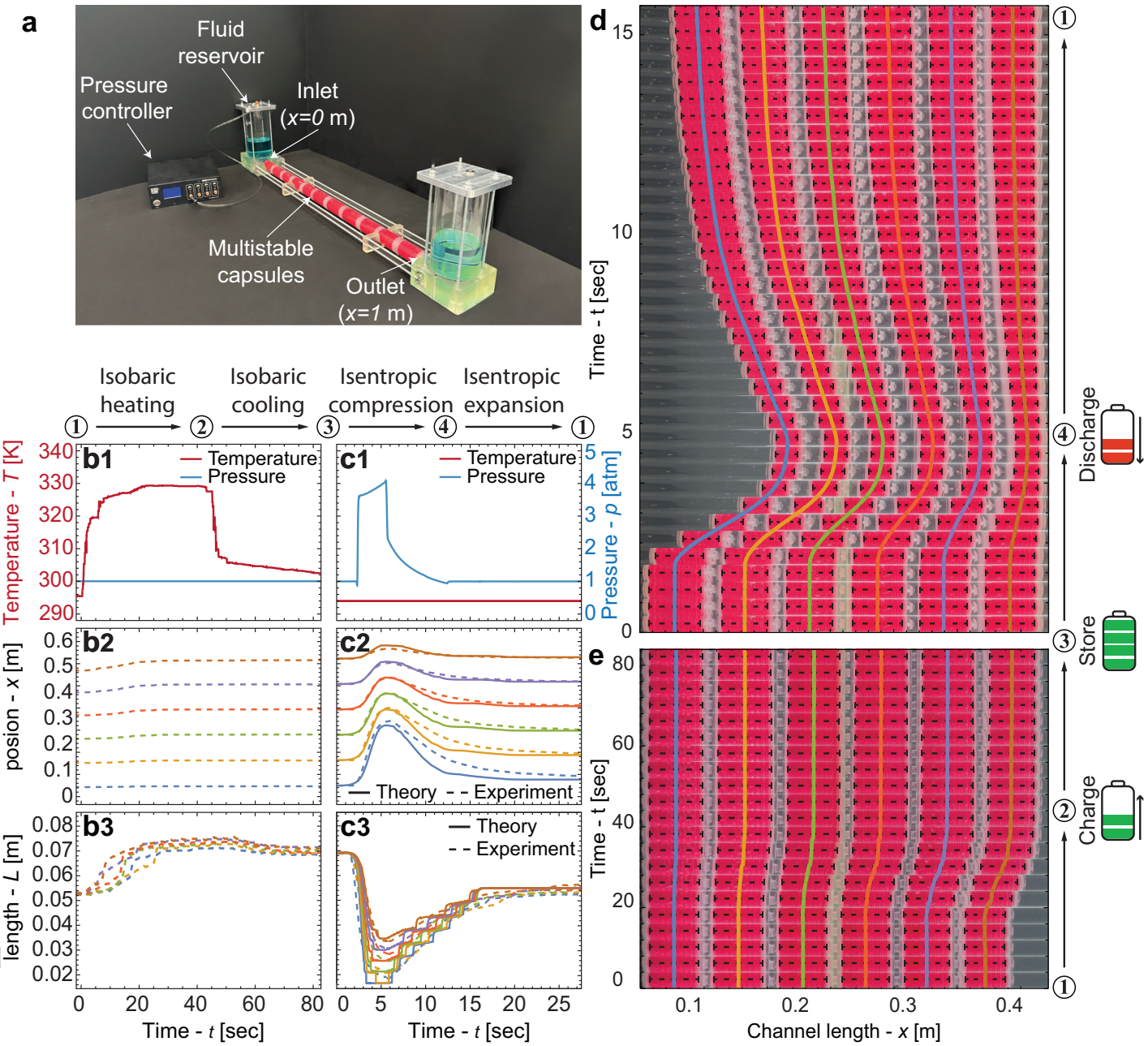

Figure 3: **Experimental results**. **a**, The experimental setup, showing the tube consisting of 1D array of capsules at initial permutation $\overrightarrow{\mathbf{per}} = \{6, 0, 12\}$ immersed within a surrounding fluid. The tube is connected to a fluidic reservoir at both ends, allowing to regulate the pressure via a pressure controller (Elvflow OB1). At the inlet (x=0), a Heaviside pressure increase is applied, which triggers a series of snap-throughs within the capsules. **b**, shows experimental results for the charging phase, including: **b1** inlet pressure measurement and temperature measured at $x = 0.5$m, **b2** capsule's center of mass location versus time, and **b3** capsules length versus time. **c**, shows experimental results for the discharging phase, including: **1** inlet pressure and temperature measurements, **c2** center of mass location ($(x_L^i + x_R^i)/2$, $i \in \{1, 2, \ldots, N\}$), and **c3** capsules length versus time. The solid lines were extracted from the analytical model and the dashed lines correspond to the experiment. **d,e**, Shows the system state at different time intervals, for the charging and discharging phases respectively, along with the video tracking result for both capsules location (solid lines) and length (black dashed lines) used to analyze the experimental results (see Supplementary Movie 1).

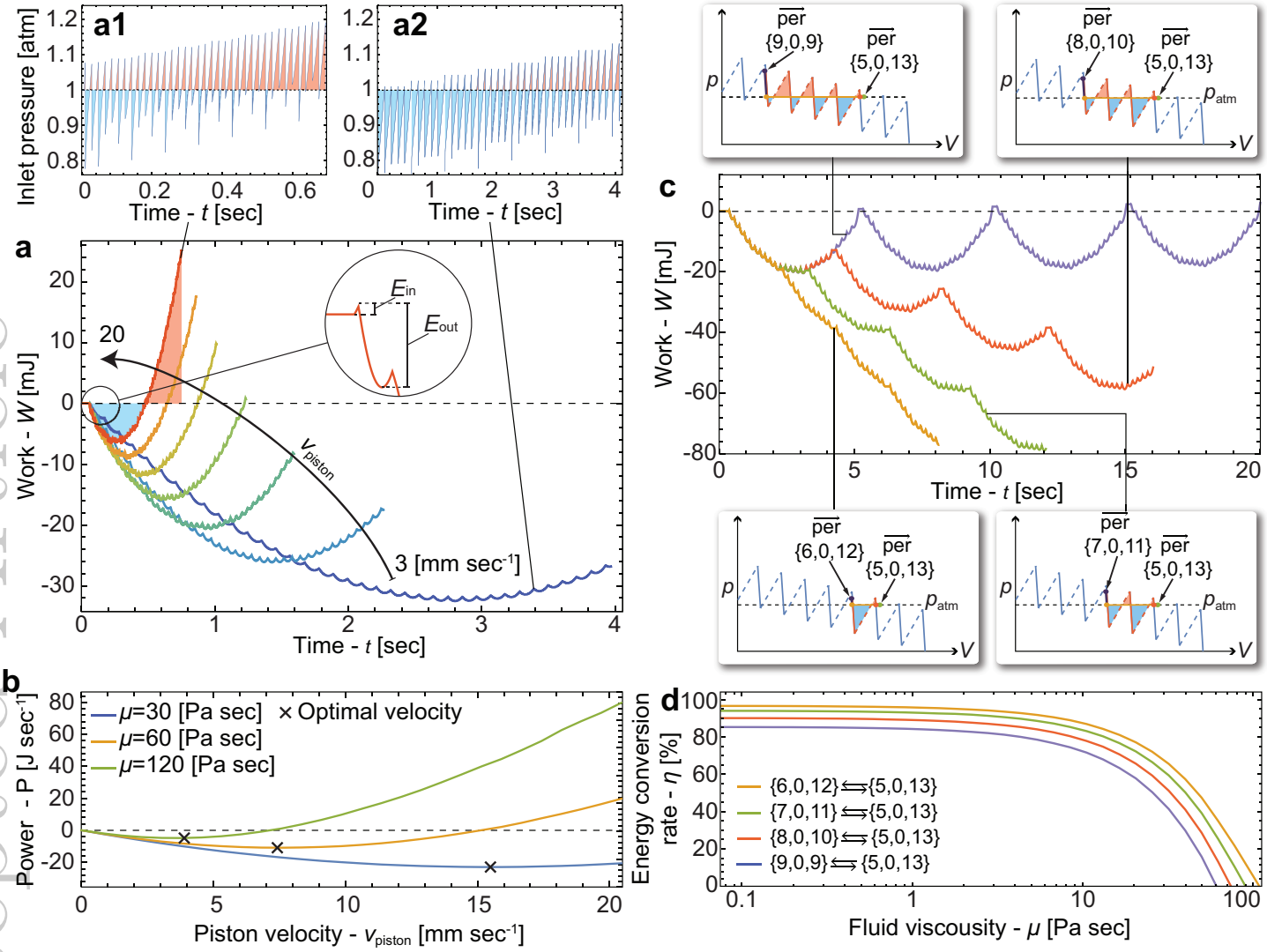

Figure 4: **Energy discharge from the Metafluid.** **a**, Work done by the piston the system in the discharging process versus time for different piston velocities. **a1,2**, Shows inlet pressure as a function of time for the case of $v_{\text{piston}} = 20$ m sec^{-1} and $v_{\text{piston}} = 3$ m sec^{-1}, respectively (blue areas denotes negative gauge pressure and and red areas denotes positive gauge pressure) **b**, Power P versus piston velocity for different viscosities of lubricating fluid. **c**, Shows net work ($W(t)$) for different initial permutations (all other parameters were maintained). **d**, Shows energy conversion rate η for different initial permutations (colors correspond to 4c) at different viscosities.

of the cycle. At state (3), the permutation is determined by the hot temperature value ($T_{\text{hot}} = 320\text{K}$), which, for the given capsule's parameters yields a single possible permutation of ($\overrightarrow{\mathbf{per}} = \{5, 0, 13\}$. The permutation in state (1) has several possible values, ranging from the atmospheric permutation $\overrightarrow{\mathbf{per}} = \{9, 0, 9\}$, to $\overrightarrow{\mathbf{per}} = \{6, 0, 12\}$. Figure 4c shows net work (W) for different initial permutations (all other parameters were maintained) for four consecutive cycles. All presented simulations start at the same permutation ($\overrightarrow{\mathbf{per}} = \{5, 0, 13\}$), and the capsules start to compress. As seen in the figure, the energy extraction rate increases as the difference between the initial and final permutations decreases.Note that the change in energy is caused by viscous friction effects. As evident from the inserts in Figure 4c, when transitioning between two permutations that are far from the atmospheric permutation, a significant improvement in energy harvesting efficiency can be observed. This is attributed to the encapsulated gas being in a higher energetic state.

2.5.2 Energy conversion rate

To assess the efficiency of the system for converting stored energy into mechanical work, we denote the energy conversion coefficient, as η. This coefficient is the ratio of energy extracted from the system during the discharging phase (W) to the total potential energy change of the system relative to its nominal state, denoted by $\Delta U = U_{state3} - U_{state1}$. The system's potential energy state, U, is a sum of the strain energy stored within the multistable structure (U_{el}), the internal gas potential energy (U_{gas}), and the work done on the system by the external force ($U_{external}$). A detailed analysis is provided in Supplementary Note 5. The energy extracted from the system is expressed by Equation 8 and is calculated for a single harvesting cycle, as illustrated in Figure 4c. Figure 4d presents the energy conversion rates calculated for varying surrounding fluid viscosities and different initial permutations (colors corresponding to those in Figure 4c). From the results, we obtain that the energy conversion rates for the experiment are $\eta = 35.1\%$, $\eta = 25.4\%$, $\eta = 13.2\%$, and $\eta = 0.23\%$ for initial permutations of $\overrightarrow{\mathbf{per}} = \{6, 0, 12\}$, $\{7, 0, 11\}$, $\{8, 0, 10\}$, $\{9, 0, 9\}$, respectively. Furthermore, the graph indicates an increase in efficiency as viscosity decreases, which can be attributed to reduced energy dissipation due to friction. The efficiency reaches values of $\eta = 85.5\%$, $\eta = 90.03\%$, $\eta = 94.27\%$, and $\eta = 95.7\%$ for viscosity values lower than 0.1 Pa sec. Thus, as expected, minimal viscosity is preferable in order to increase energy conversion in realistic applications.

3 Concluding remarks

In this work, we investigated theoretically and experimentally the fluid dynamics of a metafluid in a 1D setting. We demonstrated that a system of this kind can harvest energy from temperature fluctuations and that, due to the multistability of the metafluid, specific quanta of energy can be captured and stored indefinitely without requiring thermal isolation. This energy can then be transported as a fluid under normal atmospheric conditions.

A high-viscosity liquid was utilized in this research in order to reduce the characteristic length-scale of transient phenomena and increase the characteristic time-scale. In this way, we were able to measure transient dynamics experimentally without having to use large quantities of capsules or long containing tubes. It should be noted, however, that viscous effects should commonly be minimized to the extent possible. This study can therefore be used to estimate this phenomenon, which is unavoidable in large-scale systems that contain a large number of capsules and long tubes.

In order to realize metafluid-based energy harvesting and storage, it is necessary to fabricate multistable capsules with preferable equilibrium points, a high energy difference between these points, as well as high fatigue resistance, resulting in a long service life. The ability to manufacture large amounts of multistable capsules at a competitive price poses the greatest challenge to the distribution and commercialization of metalfluids. Upon meeting this challenge, metafluid-based energy harvesters would have a programmable operation range, allowing them to combine energy storage with energy harvesting, as well as being capable of directly harvesting energy from both positive and negative temperature changes.

4 Supporting Information

Supporting Information is available from the Wiley Online Library or from the author.

5 Acknowledgements

A.G. acknowledges support from the Israel Science Foundation grant 1285/20. S.G. acknowledges support from the Israel Science Foundation grant 1598/21. O.P acknowledges support from Israel Council for Higher Education Fellowship.

6 Data Availability Statement

The data that supports the findings of this study are available in the supplementary material of this article.

7 Conflict of Interest

The authors declare no competing interests.

References

References

[1] K. Wilkinson, C. Chissell, J. Foley, et al., *Project Drawdown* **2020**.

[2] C. Aprea, A. Greco, A. Maiorino, *Global Warming–Impacts and Future Perspective* **2012**, 41.

[3] J. M. Calm, *Int. J. Refrig.* **2002**, *25* 293.

[4] T. Noce, S. de Morais Hanriot, L. C. M. Sales, J. R. Sodre, M. B. de Novaes, *Automot. Innov.* **2020**, *3* 169.

[5] O. Peretz, E. B. Abu, A. Zigelman, S. Givli, A. D. Gat, *Nat. Commun.* **2022**, *13* 1810.

[6] K. Bertoldi, V. Vitelli, J. Christensen, M. van Hecke, *Nature Rev. Mater.* **2017**, *2* 17066.

[7] K. A. Arpin, A. Mihi, H. T. Johnson, A. J. Baca, J. A. Rogers, J. A. Lewis, P. V. Braun, *Adv. Mater.* **2010**, *22* 1084.

[8] C. M. Soukoulis, M. Wegener, *Nat. Photonics* **2011**, *5*, 9 523.

[9] S. A. Cummer, J. Christensen, A. Alù, *Nat. Rev. Mater* **2016**, *1* 16001.

[10] R. Schittny, M. Kadic, S. Guenneau, M. Wegener, *Phys. Rev. Lett.* **2013**, *110* 195901.

[11] P. Peng, C. Qiu, Y. Ding, Z. He, H. Yang, Z. Liu, *Solid State Commun.* **2011**, *151*, 5 400.

[12] M. H. Lu, L. Feng, Y. F. Chen, *Mater. Today* **2009**, *12*, 12 34.

[13] P. A. Deymier, *Springer Berlin Heidelberg. Imprint: Springer: Berlin, Heidelberg.* **2013**.

[14] D. M. Correa, T. D. Klatt, S. A. Cortes, M. R. Haberman, D. Kovar, C. C. Seepersad, *Rapid Prototyp. J.* **2015**, *21*, 2 193.

[15] D. M. Correa, C. C. Seepersad, M. Haberman, *Integr. Mater. Manuf. Innov.* **2015**, *4*, 1 10.

[16] S. Babaee, J. Shim, J. C. Weaver, E. R. Chen, N. Patel, K. Bertoldi, *Rapid Prototyp. J.* **2013**, *25*, 36 5044.

[17] X. Zheng, H. Lee, T. H. Weisgraber, M. Shusteff, J. DeOtte, E. B. Duoss, J. D. Kuntz, M. M. Biener, Q. Ge, J. A. Jackson, S. O. Kucheyev, N. X. Fang, C. M. Spadaccin, *Science* **2014**, *344*, 6190 1373.

[18] G. Puglisi, L. Truskinovsky, *J. Mech. Phys. Solids* **2000**, *48* 1.

[19] I. Benichou, S. Givli, *Extreme Mech. Lett.* **2020**, *40* 100932.

[20] C. Gao, V. Slesarenko, M. C. Boyce, S. Rudykh, Y. Li, *Sci. Rep.* **2018**, *8*, 1 1.

[21] Y. Chen, L. Jin, *Adv. Funct. Mater.* **2021**, *31*, 31 2102113.

[22] F. Pan, Y. Li, Z. Li, J. Yang, B. Liu, Y. Chen, *Adv. Mater.* **2019**, *31*, 25 1900548.

[23] S. Katz, S. Givli, *Extreme Mech. Lett.* **2018**, *22* 106.

[24] S. Katz, S. Givli, *EPL (Europhysics Letters)* **2020**, *131*, 6 64002.

[25] A. Guell Izard, L. Valdevit, *Adv. Eng. Mater.* **2020**, *22*, 2 1901019.

[26] H. Fan, Y. Tian, L. Yang, D. Hu, P. Liu, *Mech. Adv. Mater. Struct.* **2022**, *29*, 11 1637.

[27] F. Liu, Z. Wang, M. Ke, Z. Liu, *Phys. Rev. Lett.* **2020**, *125* 185502.

[28] E. Epstein, J. Yoon, A. Madhukar, K. J. Hsia, P. V. Braun, *Small* **2015**, *11*, 45 6051.

[29] W. Zhang, Q. Song, W. Zhu, Z. Shen, P. Chong, D. P. Tsai, C. Qiu, A. Q. Liu, *Adv. Phys.: X* **2018**, *3*, 1 1417055.

[30] N. P. Bende, T. Yu, N. A. Corbin, M. A. Dias, C. D. Santangelo, J. A. Hanna, R. C. Hayward, *Soft Matter* **2018**, *14*, 42 8636.

[31] Y. Liu, F. Pan, B. Ding, Y. Zhu, K. Yang, Y. Chen, *Extreme Mech. Lett.* **2022**, *50* 101535.

[32] B. Ni, H. Gao, *Journal of Applied Mechanics* **2020**, *87*, 3 031012.

[33] Z. Wo, E. T. Filipov, *Journal of Applied Mechanics* **2022**, *89*, 4 041005.

[34] T. Cohen, S. Givli, *J. Mech. Phys. Solids* **2014**, *64* 426.

[35] I. Benichou, E. Faran, D. Shilo, S. Givli, *Appl. Phys. Lett.* **2013**, *102*, 1 011912.